Comb-Like Fluorophilic-Lipophilic-Hydrophilic Polymers for Nanocapsules as Ultrasound Contrast Agents

Sophie Houvenagel, Laurence Moine, Guilherme Picheth, Camille Dejean, Annie Brûlet, Alexis Chennevière, Vincent Faugeras, Nicolas Huang, Olivier Couture, Nicolas Tsapis

Comb-like fluorophilic-lipophilic-hydrophilic polymers for nanocapsules as ultrasound contrast agents

Sophie Houvenagel[a], *Laurence Moine*[a]*, *Guilherme Picheth*[a], *Camille Dejean*[b], *Annie Brûlet*[c], *Alexis Chennevière*[c], *Vincent Faugeras*[d], *Nicolas Huang*[a], *Olivier Couture*[d], *Nicolas Tsapis*[a]*

[a] Institut Galien Paris-Sud, CNRS, Univ. Paris-Sud, Université Paris-Saclay, 92296 Châtenay-Malabry, France

[b] BioCIS, CNRS, Univ. Paris-Sud, Université Paris-Saclay, 92296 Châtenay-Malabry, France

[c] Laboratoire Léon Brillouin, UMR12 CEA-CNRS, CEA Saclay, Gif sur Yvette, F-91191, France

[d] Institut Langevin, ESPCI Paris, CNRS (UMR 7587), INSERM (U979), Paris, France

* Corresponding authors at: CNRS, Institut Galien Paris-Sud, CNRS UMR 8612, Faculté de Pharmacie, 92296 Châtenay-Malabry, France. E-mail address: laurence.moine@u-psud.fr (Laurence Moine) and nicolas.tsapis@u-psud.fr (Nicolas Tsapis)

Keywords

Comb-like fluorinated polymers; fluorous interactions; nanocapsules; perfluorocarbons; ultrasound contrast agents

Abstract

Imaging the enhanced permeation and retention effect by ultrasound is hindered by the large size of commercial ultrasound contrast agents (UCAs). To obtain nanosized UCAs, triblock copolymers of poly(ethylene glycol)-polylactide-poly(1H,1H,2H,2H-heptadecafluorodecyl methacrylate) (PEG-PLA-PFMA) with distinct numbers of perfluorinated pendant chains (5, 10 or 20) are synthesized by a combination of ring-opening polymerization and atom transfer radical polymerization. Nanocapsules (NCs) containing perfluorooctyl bromide (PFOB) intended as UCAs are obtained with a 2-fold increase in PFOB encapsulation efficiency in fluorinated NCs as compared to plain PEG-PLA NCs thanks to fluorous interactions. NC morphology is strongly influenced by the number of perfluorinated chains and the amount of polymer used for formulation, leading to peculiar capsules with several PFOB cores at high PEG-PLA-PFMA$_{20}$ amount and single-cored NCs with a thinner shell at low fluorinated polymer amount, as confirmed by small angle neutron scattering. Finally, fluorinated NCs yield higher in vitro ultrasound signal compared to PEG-PLA NCs and no in vitro cytotoxicity is induced by fluorinated polymers and their degradation products. Our results highlight the benefit of adding comb-like fluorinated blocks in PEG-PLA polymers to modify the nanostructure and enhance the echogenicity of nanocapsules intended as UCAs.

1. Introduction

Ultrasound is one of the most widely used clinical imaging modality owing to its low cost, safety, portability, and possible combination with therapy.[1] Nevertheless, this technique has been limited by the lack of effective ultrasound contrast agents (UCAs) to allow tissue differentiation.[2,3] Commercially available UCAs consist of 1 – 6 μm gas microbubbles stabilized by a layer of lipids or proteins.[4,5] Their large size and high compressibility make them ideal ultrasound reflectors, currently used to enhance the blood pool signal and assess tissue blood flow at the microvascular level.[6] However, the fast diffusion of the encapsulated gas results in short circulation time in the bloodstream (a few minutes),[7] and their large micrometer size prevents their accumulation in solid tumors. For tumor imaging, more stable nano-sized UCAs able to extravasate into tumors by the enhanced permeation and retention (EPR) effect[8] are required. Since gas nanobubbles are difficult to stabilize,[9] research has focused on the encapsulation of liquid perfluorocarbons.[10] To further improve UCAs stability, several groups have reported the use of polymeric shells which are more stable than lipid or protein layers.[11–14]

In this context, polymeric UCAs have been developed recently in our group. These polymeric nanocapsules (NCs) of poly(lactide-co-glycolide) (PLGA) encapsulating liquid perfluorooctyl bromide (PFOB) showed long-lasting *in vitro* echogenicity and allowed *in vivo* blood pool imaging.[15] However, quick elimination by the mononuclear phagocyte system hampered their accumulation in the tumor. PLGA was then replaced by poly(lactide-co-glycolide)-poly(ethylene glycol) (PLGA-PEG) copolymer to formulate long-circulating NCs which accumulated in the tumor by the EPR effect, and yielded contrast enhancement by ^{19}F Magnetic Resonance Imaging.[16] Nevertheless, the acoustic response of these capsules remained too weak at clinical frequencies, owing mainly to the important thickness of their shells. The strategy of decreasing the polymer amount in the formulation, which previously

allowed reducing the thickness of plain PLGA NCs,[17] failed using PLGA-PEG due to local dewetting.[18]

Our aim is therefore to improve the nanocapsule echogenicity by reducing their shell thickness, while keeping their long-circulating properties with PEG chains. Recently, we reported that functionalizing PLA with a short linear perfluorinated end group induced an increase of PFOB encapsulation efficiency into PEGylated NCs made of a mixture of PLA-PEG and fluorinated-PLA, for perfluorinated chain length up to C_8F_{17}.[19] However, the shell thickness was not reduced, and although a higher *in vitro* echogenicity was obtained due to fluorination, there is still room for improvement since the ultrasound signal was much lower than commercial Sonovue microbubbles.

Plenty of reports on different triblock copolymers with hydrophilic, hydrophobic, and fluorinated blocks exist and nanoparticles formed using these polymers exhibit different morphologies.[20–24] Here, the strategy consists in synthesizing triblock hydrophilic-hydrophobic-fluorophilic copolymers of poly(ethylene glycol)-polylactide-poly(1H,1H,2H,2H-heptadecafluorodecyl methacrylate) (PEG-PLA-PFMA), containing a higher proportion of C_8F_{17} chains, to formulate nanocapsules. We intend to favor fluorous interactions between the fluorinated chains and PFOB to improve the wetting of the polymer around the PFOB core and yield capsules with thin shells as we decrease the amount of polymer in the formulation. We present here the polymer synthesis and the characterization of nanocapsules in terms of size distribution, morphology, PFOB encapsulation efficiency, shell thickness as measured by Small Angle Neutron Scattering, cytotoxicity and *in vitro* ultrasound scattering.

2. Materials and methods

2.1. Materials

DL-lactide was purchased from Biovalley, Polysciences Inc. (USA). Poly(ethylene glycol) methyl ether (OH-PEG-OCH_3, average M_n = 5 000 g/mol), stannous 2-ethyl hexanoate (stannous octoate, $Sn(Oct)_2$), N,N,N′,N″,N″-pentamethyldiethylenetriamine (PMDETA), triethylamine (Et_3N), dried toluene, cyclohexanone, magnesium sulfate ($MgSO_4$), sodium cholate, D_2O and trifluoroacetic acid (TFA) were provided by Sigma-Aldrich (France). 1H,1H,2H,2H-heptadecafluorodecyl methacrylate (FMA) and perfluorooctyl bromide (PFOB) were purchased from Fluorochem (UK). 2-Bromo-2-methylpropionyl bromide and copper(I) bromide (CuBr) were provided by ACROS Organics (Belgium). Deuterated chloroform ($CDCl_3$) was obtained from Euriso-top (France). All solvents were purchased from Carlo Erba (France). Cell culture reagents such as DMEM (Dulbecco's modified Eagle's medium), RPMI 1640 (Roswell Park Memorial Institute medium), FBS (Fetal Bovine Serum), trypsin-EDTA solution and PBS (Ca^{2+} and Mg^{2+} free phosphate buffer) were purchased from Sigma Aldrich (France). Water was purified using a RIOS/Synergy system from Millipore (France). NMR sample tubes and coaxial inserts were obtained from CortecNet (France).

2.2. Polymer synthesis

The synthesis route involved 3 steps as shown in Figure 1.

2.2.1. Synthesis of PEG-PLA

PEG-PLA was synthesized by ring-opening polymerization (ROP) of DL-lactide initiated by OH-PEG-OCH_3 in the presence of stannous octoate catalyst.[25] All glassware was dried by heating under vacuum and handled under argon atmosphere. To a 250 mL round-bottom flask equipped with a magnetic stir-bar were added DL-lactide (156.14 mmol, 22.50 g) and OH-PEG-OCH_3 (1.13 mmol, 5.66 g). The flask was sealed with a rubber cap and a stannous

112 octoate solution (0.75 mmol, 306 mg) dissolved in 30 mL of dried toluene was added through
113 the septum. The tube was purged with argon for 15 minutes and then placed into a 130°C oil
114 bath. Polymerization was carried out for 1h under magnetic stirring, and then quenched by
115 immersing the tube in a cold water bath. After evaporation of toluene, the reaction product
116 was dissolved in chloroform and precipitated twice into excess cold diethyl ether. The
117 polymer was finally dried under vacuum and 25.13 g of a white powder was obtained. Lactide
118 conversion = 94% (^{1}H NMR). ^{1}H NMR (300 MHz, $CDCl_3$, δ, ppm): 5.10-5.28 (C*H*CH_3COO
119 of PLA), 3.64 (OCH_2CH_2 of PEG), 3.38 (OCH_3 of PEG), 2.70 (end *H*OCHCH_3COO of PLA),
120 1.45-1.67 (CHCH_3COO of PLA). M_n^{NMR} = 23,500 g/mol; M_n^{SEC} = 24,300 g/mol.

121 2.2.2. Synthesis of PEG-PLA-Br macroinitiator

122 PEG-PLA-Br was synthesized by esterification of PEG-PLA with excess 2-Bromo-2-
123 methylpropionyl bromide using a known procedure.[26,27] In a 250 mL round-bottom flask
124 equipped with a magnetic stir-bar, PEG-PLA (1.06 mmol, 25 g) was dissolved in 160 mL of
125 CH_2Cl_2. Excess of triethylamine (37.23 mmol, 5.2 mL) was added to the solution, and the
126 mixture was stirred under argon and cooled to 0°C with an ice bath. 2-Bromo-2-
127 methylpropionyl bromide (37.23 mmol, 4.6 mL) was added dropwise for 15 min. The mixture
128 was allowed to stir at room temperature overnight, and was subsequently washed twice with
129 saturated brine and once with water. The organic phase was dried over anhydrous $MgSO_4$
130 before being concentrated under reduced pressure and precipitated twice in excess cold
131 diethyl ether. The product was finally dried under vacuum to provide 16.55 g of an off-white
132 solid. ^{1}H NMR (300 MHz, $CDCl_3$, δ, ppm): 5.10-5.28 (C*H*CH_3COO of PLA), 3.64
133 (OCH_2CH_2 of PEG), 3.38 (OCH_3 of PEG), 1.95 and 1.98 (C(Br)(CH_3)$_2$), 1.45-1.67
134 (CHCH_3COO of PLA). M_n^{NMR} = 23,500 g/mol; M_n^{SEC} = 25,200 g/mol.

2.2.3. Synthesis of PEG-PLA-PFMA$_x$ polymers

PEG-PLA-PFMA$_x$ polymers were synthesized by ATRP of 1H,1H,2H,2H-heptadecafluorodecyl methacrylate (FMA) initiated by PEG-PLA-Br with CuBr/PMDETA as the catalyst system.[28] All glassware was dried by heating under vacuum and handled under argon atmosphere. To a 100 mL round-bottom flask equipped with a magnetic stir-bar were added PEG-PLA-Br (0.21 mmol, 5 g) and a solution of PMDETA (0.21 mmol, 37 mg) and FMA (1.06 mmol for x = 5, 2.13 mmol for x = 10, 4.26 mmol for x = 20) in cyclohexanone (15 mL). After dissolution of the macroinitiator, CuBr (0.21 mmol, 31 mg) was added and the mixture was subjected to two freeze-pump-thaw cycles. The reaction proceeded at 100 °C for 42h. The mixture was cooled and diluted with THF, and the copper catalyst was removed with a neutral alumina column. After concentration under reduced pressure, the product was precipitated twice in excess cold diethyl ether and dried under vacuum. FMA conversion (^{1}H NMR) = 84% (x = 20), 80% (x = 10), 67% (x = 5). ^{1}H NMR (300 MHz, $CDCl_3$, δ, ppm): 5.10-5.28 (C*H*CH_3COO of PLA), 4.28 (OC*H*$_2$$CH_2$$CF_2$ of PFMA), 3.64 (OC*H*$_2$C*H*$_2$O of PEG), 3.38 (end OC*H*$_3$ of PEG), 2.47 (OCH_2C*H*$_2$$CF_2$ of PFMA), 1.70-2.00 (C*H*$_2$C(CH_3)COO of PFMA), 1.45-1.67 (CHC*H*$_3$COO of PLA), 0.80-1.45 (CH_2C(C*H*$_3$)COO of PFMA). Molar masses are displayed in Table 1.

2.3. Polymer characterization

Size exclusion chromatography (SEC) was performed at 30 °C with two columns from Polymer Laboratories (PL-gel MIXED-D; 300 × 7.5 mm) and a differential refractive index detector (Spectrasystem RI-150, Thermo Electron Corp.), using chloroform as an eluent, a Waters 515 pump at a flow rate of 1 mL/min, and toluene as a flow-rate marker. The polymers were dissolved at 5 mg/mL in the eluent and filtered on 0.2 µm PTFE syringe filters prior to injection. The calibration curve was based on poly(methyl methacrylate) (PMMA) standards from Polymer Laboratories. ^{1}H NMR and ^{19}F NMR spectroscopies were performed

in 5 mm diameter tubes in $CDCl_3$ on a Bruker Avance-400 (400 MHz) spectrometer. The DP and M_n of the commercial OH-PEG-OCH_3 were confirmed by ^1H NMR in $CDCl_3$ using the ratio of the methyl signal at 3.38 ppm versus the main chain signal at 3.64 ppm: DP = 118, M_n = $5.2x10^3$ g/mol. Differential scanning calorimetry (DSC) was performed using a DSC Q1000 (TA Instruments). The polymers (2-5 mg) were sealed in aluminum pans and heated from -20 to 100°C at a heating rate of 20°C/min and cooled to -20 °C before a second heating scan from -20 to 100°C at 20°C/min to determine the glass transition temperature (T_g). A nitrogen flow was maintained throughout the test (20 mL/min).

2.4. Interfacial tension measurements

Interfacial tension measurements were carried out using the pendant drop method, employing a Tracker tensiometer (Teclis, France). Drops of PFOB were formed using a syringe and a G22 stainless steel needle into a methylene chloride solution containing the polymers at 25 mg/mL placed in an optical glass cuvette. The interfacial tension was determined from the drop profile using the Laplace equation and the forces balance between capillarity and gravity. The measurements were performed on at least three independent drops and the experiment was repeated on different days to ensure reproducibility.

2.5. Nanocapsules preparation

Nanocapsules (NCs) of PFOB were prepared by an emulsion-evaporation process as previously described.[16,19] The polymer (50, 30 or 20 mg) was dissolved into 2 mL of methylene chloride along with 30 µL of PFOB. The organic phase was emulsified into 10 mL of 1.5 % sodium cholate (w/v) aqueous solution using a vortex for 1 min and then a vibrating metallic tip (Digital Sonifier, Branson Ultrasons, France) at 30% of maximal power, for 1 min over ice. Solvent was allowed to evaporate by magnetic stirring at 300 rpm at room temperature for 3 h. Suspensions of NCs were filtered through 0.45 µm PVDF filters, and if

necessary, were purified to remove sodium cholate by ultracentrifugation for 1h, at 4 °C and at 27 440 g (Optima LE-80K Ultracentrifuge Beckman Coulter). The pellet was finally resuspended in water to the desired concentration.

2.6. Size distribution and Zeta potential

The hydrodynamic diameter (d_H) and polydispersity index (PDI) of the nanocapsules were measured by quasi-elastic light scattering, using a Zetasizer Nano ZS instrument (Malvern, France). Suspensions were diluted in water to a concentration of 1 mg/mL. Measurements were performed at 20 °C, at an angle of 173° to avoid multiple scattering. Zeta potential measurements were carried out with the same instrument, at 25 °C, in 1 mM NaCI. Measurements were performed in triplicate.

2.7. PFOB encapsulation efficiency by ^{19}F NMR spectroscopy

PFOB encapsulation efficiency was determined by ^{19}F NMR on a Bruker Avance-400 (400 MHz) spectrometer with a 5 mm dual probe ^{19}F/^{1}H. The NMR quantitative method using stem coaxial inserts was originally proposed by Henderson for ^{31}P compounds[29] and adapted previously for ^{19}F NMR.[30,19] 1 mL of unpurified nanocapsules were freeze-dried for 24h using an Alpha-1-2 LD apparatus (Christ, France) and lyophilisates were dissolved into 1 mL of chloroform. Sodium cholate was removed by centrifugation for 5 min at 4696 g. The organic solution was collected and introduced into a usual 5mm-NMR sample tube loaded with a stem coaxial insert containing TFA in D_20 as an external standard ([TFA]= 9.4 µmol.mL^{-1}). The total amount of PFOB in the suspension, n_{PFOB}, was determined after integration of the peak at -64.7 ppm corresponding to the CF_2Br group and normalization by the area of the TFA peak at -76.5 ppm. Absolute encapsulation efficiency, η_{encaps}, was calculated as follows:

$$\eta_{encaps} = \frac{n_{PFOB}}{n_{PFOB}^{max}} \text{ with } n_{PFOB}^{max} = \frac{m_{PFOB}^{feed}}{M_{PFOB}} \frac{m_{NC}}{m_{PFOB}^{feed} + m_{polymer}^{feed} + m_{SC}^{feed}}$$

where m_{PFOB}^{feed}, $m_{polymer}^{feed}$ and m_{SC}^{feed} are the initial masses of the components introduced during NCs preparation, m_{NC} corresponds to the mass of NCs recovered after freeze-drying and M_{PFOB} is the molar mass of PFOB (498.96 g/mol).

2.8. Transmission electron microscopy (TEM)

TEM was performed at I2BC (Gif-sur-Yvette, France) using a JEOL JEM-1400 operating at 80 kV. 5 µL of purified suspensions of nanocapsules (0.5 mg/mL) were deposited for 1 min on glow-discharged copper grids covered with formvar-carbon film. Samples were then stained using 2% phosphotungstic acid (pH = 7) for 30 s. The excess solution was blotted off using a filter paper. Images were acquired using an Orius camera (Gatan Inc, USA).

2.9. Cryo-transmission electron microscopy (cryoTEM)

CryoTEM was performed at I2BC (Gif-sur-Yvette, France) using a JEOL JEM-1400 operating at 120 kV. 5 µL of purified suspensions of nanocapsules (25 mg/mL) were deposited on glow-discharged Lacey copper grids covered with carbon film containing holes. The excess solution was blotted off for 5 s using filter paper and the grids were subsequently frozen in liquid ethane using a Leica EM GP automatic system (Leica, Austria) under a 90% humidity atmosphere. Images were recorded on a US1000XP camera (Gatan Inc, USA) with a -2 µm defocus.

2.10. Small angle neutrons scattering (SANS)

2.10.1. SANS data collection

Small Angle Neutron Scattering (SANS) measurements were performed on the PACE spectrometer of the Laboratoire Léon Brillouin (LLB, CEA-Saclay, France). Nanocapsules

were filtered, purified and resuspended at a final volume fraction of φ_v = 1% in a 40/60 (v/v) H_2O/D_2O mixture to match the scattering length density of the PFOB core ($\rho_{PFOB} = \rho_{core}$ = 3.6 x 10^{10} cm^{-2}). This mixture has a weak contrast with PFMA block polymer (ρ_{PFMA} = 3.0 x 10^{10} cm^{-2}). So, using contrast matching of the PFOB core, we focused on the polymeric shell of PEG-PLA blocks. Two configurations were used: the first one with a sample-to-detector distance of D = 4.7 m and a neutron wavelength of λ = 13 Å and the second one with D = 2.9 m and λ = 4.6 Å to cover a broad q range of $3.2 \times 10^{-3} – 1.5 \times 10^{-1}$ $Å^{-1}$. SANS measurements were performed in 1 mm thick quartz cuvettes to minimize the incoherent scattering. Scattered intensity curves were corrected from the scattering from the empty quartz cuvette and the electronic background, and normalized by the incoherent signal of 1 mm water sample to account for non-uniform efficiency of detector, using the LLB PASINET software.[31]

2.10.2. SANS data modelling

The scattered intensity curves obtained in PFOB matching condition were fitted using the vesicle model with Sasview software.[32] This model provides the form factor, P(q), for a unilamellar vesicle of inner radius R_{core} and thickness T, according to the following equation:

$$P(q) = \frac{scale}{V_2}\left[\frac{3V_1(\rho_1 - \rho_2)\,J_1(qR_1)}{qR_1} + \frac{3V_2(\rho_2 - \rho_{solv})\,J_1(qR_2)}{qR_2}\right]^2$$

Where scale is a scale factor, V_1 is the volume of the core, V_2 is the total volume of the vesicle, $R_1 = R_{core}$ is the radius of the core, R_2 is the outer radius of the vesicle ($R_2 = R_{core}$ + T), and $J_1(x) = \frac{\sin x - x\cos x}{x^2}$. For the vesicle, $\rho_1 = \rho_{core} = \rho_{solv}$ is the scattering length density of the core and the solvent, $\rho_2 = \rho_{shell}$ is the scattering length density of the shell. The fit gives geometrical parameters of the nanocapsules: the mean core radius R_{core}, the polydispersity of the core radius σ_{core}, the thickness of the shell T and the polydispersity of the thickness σ_T. A lognormal distribution was assumed for both radius and thickness.

2.11. Hydrolytic degradation of polymers

50 mg of each polymer (except PEG-PLA-$PFMA_{20}$) were suspended into 1 mL of NaOH 1M and vigorously stirred for 24h at 37°C in an incubator. After adjustment of the pH to 7 with HCl 1M, the cloudy solution was dialyzed against deionized water for 96h to remove salt and lactic acid (dialysis membrane molecular weight cut off: 100–500 Da).

2.12. Cell culture

Human endothelial umbilical vein cells (HUVEC) obtained from ATCC (USA) were cultured in DMEM supplemented with 50 $U.mL^{-1}$ penicillin, 50 $U.mL^{-1}$ streptomycin, and 10% heat inactivated FBS. The J774.A1 murine macrophage monocyte cell line (ATCC, USA) was cultured in RPMI 1640 medium supplemented with 50 $U.mL^{-1}$ penicillin, 50 $U.mL^{-1}$ streptomycin, and 10% heat inactivated FBS. Cells were split twice a week, by trypsinisation for HUVEC and by scraping for J774.A1 cells. All cell lines were maintained at 37 °C and 5% CO_2 under a humidified atmosphere.

2.13. Cytotoxicity evaluation of NCs and polymer degradation products

To evaluate their *in vitro* cytotoxicity, NCs and polymer degradation products were diluted in cell culture medium before being added onto the cells. The cell viability was evaluated using the 3-[4,5-dimethylthiazol-2-yl]-3,5-diphenyltetrazolium bromide (MTT) assay. Briefly, cells were seeded in 100 µL of culture medium (12×10^3 cells/well or 3×10^3 cells/well for 24 and 72h incubation respectively) in 96 well plates (TPP, Switzerland) and pre-incubated for 24 h. 100 µL of a serial dilution of NCs (0.01 to 10 mg/mL) or of polymer degradation products (10^{-5} to 0.01 mg/mL of initial polymer) was then added to the medium. After 24 or 72h of incubation, the incubation medium was replaced by fresh medium containing 0.5 mg/mL of MTT (Sigma, France). After 1h incubation, the culture medium was gently aspirated and replaced by 200 µL dimethylsulfoxide (ACS grade, VWR, France) to dissolve the formazan

crystals. The absorbance of the solubilized dye, which correlates with the number of living cells, was measured with a microplate reader (LAB Systems Original Multiscan MS, Finland) at 570 nm. The percentage of viable cells in each well was calculated as the absorbance ratio between treated and untreated control cells.

2.14. *In vitro* ultrasound measurements

Suspensions of nanocapsules (1 mL, 5 mg/mL) were placed in a 10 mm x 10 mm x 45 mm polystyrene cuvette in which 5-mm diameter holes were cut out and covered by acoustically transparent mylar membrane, as shown in Figure S1. The cuvette was placed in a water bath at 37°C, and a small magnetic bar allowed agitating gently the suspension without disturbing the signal. Measurements were performed after 4 minutes to allow temperature equilibration and removal of potential bubbles. A Handyscope HS5 (TiePie engineering, Netherlands) was used as both an arbitrary wave generator and a USB oscilloscope connected to a computer using Matlab (Mathworks, USA). Samples were insonified by a transducer (focal length 51 mm, model I3-0506-R-SU-F2.00IN, Olympus, France), which emitted 10 bursts of 500 cycles at 5 MHz. The scattered ultrasound signal was received by a second transducer (focal length 51 mm, model I3-1506-R-SU-F2.00IN, Olympus, France) placed at a 90° angle compared to the transducer-transmitter (Figure S1). This scattered signal was preamplified before being measured by the oscilloscope connected to Matlab for signal processing. The signal was then windowed, Fourier-transformed and the scattered intensity within the bandwidth of each harmonics was summed. The resulting ultrasound scattered intensities were subtracted from the intensity obtained with the cuvette filled with Milli-Q water. At least 9 measurements were performed with each sample. Commercial SonoVue® microbubbles (diluted to 1/1000) were used as a reference positive control for the ultrasound set-up and parameters chosen for our study.

3. Results and discussion

3.1. Polymers synthesis and characterization

Triblock copolymers carrying perfluoroalkyl pendant chains were synthesized by a combination of ROP and ATRP as shown in Figure 1.

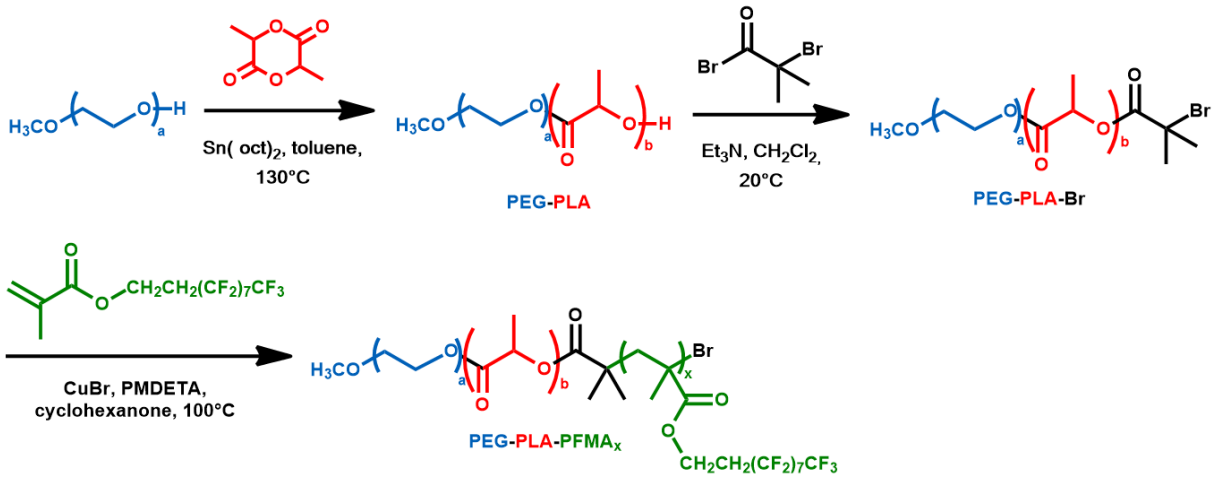

Figure 1. Synthesis of PEG-PLA-PFMA$_x$ triblock copolymers.

ROP of D,L-lactide with polyethylene glycol methyl ether (M_n = 5,000 g/mol) as initiator and Sn(oct)$_2$ as catalyst first led to PEG-PLA diblock copolymer with molar mass close to the targeted M_n of 25,000 g/mol (M_n^{NMR} = 23,500 g/mol, M_n^{SEC} = 25,500 g/mol). PEG-PLA was subsequently converted to PEG-PLA-Br macroinitiator through esterification with excess 2-bromo-2-methylpropionyl bromide in the presence of triethylamine. Quantitative conversion was confirmed by ^{1}H NMR with disappearance of the end hydroxyl broad signal of PLA at 2.70 ppm and appearance of signals at 1.95 and 1.98 ppm corresponding to the methyl protons from 2-bromo-2-methylpropionyl end group (supplementary material Figure S2).

The final PEG-PLA-PFMA$_x$ copolymers were prepared by ATRP of FMA in cyclohexanone with PEG-PLA-Br as macroinitiator and CuBr/PMDETA complex as catalyst. The nature and amount of solvent were initially varied to achieve final polymerization with satisfactory conversion (>65%). Three different monomer/initiator feed molar ratios (x = 5, 10, 20) were

used to design polymers with various fluorinated block lengths. Successful polymerization was confirmed by ^{1}H NMR with appearance of the signals at 2.47 and 4.28 ppm corresponding respectively to CH_2CF$_2$ and CH_2CH$_2$CF$_2$ protons of the PFMA block (signals h and g, Figure 2), in addition to those of the methacrylate backbone 1.70 – 2.00 and 0.80 – 1.45 (signals e and f, Figure 2). The 4.28 ppm peak area was used to calculate the copolymer molar composition and molar mass by normalization with the 3.64 ppm peak corresponding to the OCH_2CH_2 of PEG (Table 1).

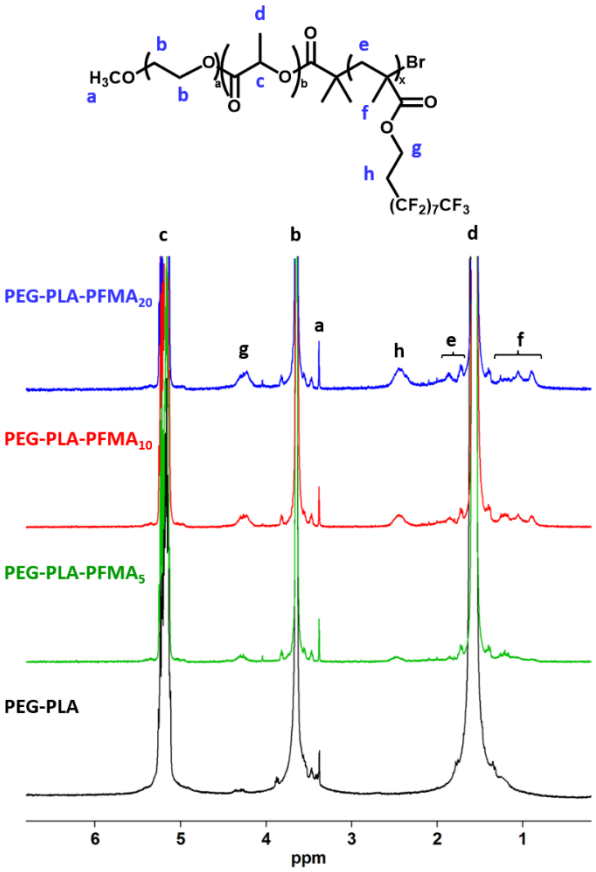

Figure 2. ^{1}H NMR spectra of PEG-PLA and triblock copolymers PEG-PLA-PFMA$_x$ in $CDCl_3$ (normalized with the PEG peak at 3.64 ppm).

^{19}F NMR spectra of all polymers further support the successful polymerization of FMA (Figure 3). A broadening of the fluorine resonances is observed in PEG-PLA-PFMA$_5$ spectrum as compared to the monomer. This effect is more pronounced as the number of

perfluoroalkyl pendants increases, and leads to the overlapping of resonances of CF_2 groups b' in PEG-PLA-PFMA$_{10}$ and PEG-PLA-PFMA$_{20}$ spectra, in agreement with previous reports.[33,34] Moreover, a splitting of the peaks c' and d', corresponding to the CF_2 and CF_3 groups at the extremity of the fluorinated pendants, is observed. This suggests the existence of unaveraged conformations and therefore indicates some degree of self-association in chloroform.

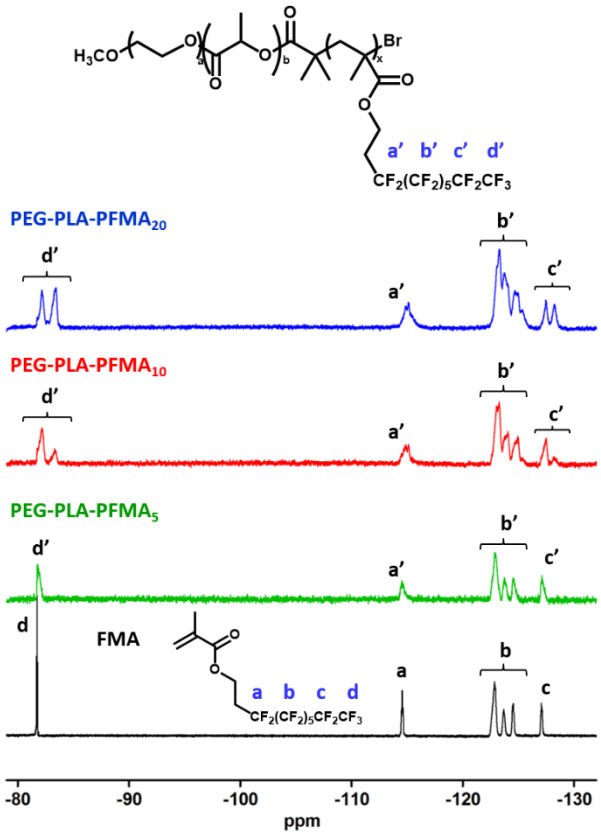

Figure 3. ^{19}F NMR spectra of FMA (black line) and triblock copolymers PEG-PLA-PFMA$_x$ in $CDCl_3$.

The molar masses were also determined by conventional SEC in chloroform (Table 1). All polymers present a single peak (supplementary material Figure S3), confirming the successful formation of copolymers rather than homopolymer blends. Although M_n^{SEC} values are close to M_n^{NMR} values, M_n^{SEC} does not increase with the polymerization degree of the PFMA block, as shown by the superposition of chromatograms and the values in the 24,000 – 26,500 g/mol

range. Because of fluorophilicity of the perfluorinated chains, full swelling of the triblock polymers in chloroform is limited by a probable folding or formation of micellar domains. Indeed, the triblock polymers appeared more difficult and longer to solubilize than non-fluorinated PEG-PLA in common organic solvents such as chloroform, methylene chloride and acetone. To confirm this different behavior, DLS analysis of fluorinated polymers at 25 mg/mL in methylene chloride and chloroform was performed. It revealed an important increase of scattered intensity compared to plain PEG-PLA (around 15000 kcps for the triblocks compared to 200 kcps for PEG-PLA, see supplementary material Figure S4). This indicates presence of aggregates such as micelles which confirms that the fluorinated block strongly impacts the solubility and conformation of the polymers chains.

Table 1. Degree of polymerization (DP), number-average molar mass (M_n), dispersity ($Đ$) and glass transition temperature (T_g) of PEG-PLA-PFMA$_x$ polymers and their precursors.

Polymer	$M_n^{theoretical}$ (x 10^3 g/mol)	DP PLA:PFMA[1]	M_n^{NMR} (x 10^3 g/mol)	M_n^{SEC} (x 10^3 g/mol)	$Đ$	T_g (°C)
PEG-PLA	25.0	257	23.5	24.3	1.29	13 ± 1
PEG-PLA-Br	25.0	260	23.7	25.2	1.28	ND
PEG-PLA-PFMA$_5$	27.7	272:4	26.7	25.0	1.38	16 ± 1
PEG-PLA-PFMA$_{10}$	30.3	291:7	29.7	24.9	1.39	20 ± 2
PEG-PLA-PFMA$_{20}$	35.6	277:15	32.9	26.2	1.29	18 ± 1

[1]The DP and M_n^{NMR} were determined from the areas of the peak at 3.64 ppm (OCH_2CH_2 of PEG) versus 5.19 ppm (C*H* of PLA) for PLA, and versus 4.28 ppm (CH_2CH$_2$CF$_2$ of PFMA) for PFMA.

DSC thermograms of all polymers exhibited a single glass transition temperature (T_g) in the 16-20°C range for triblock copolymers, slightly higher than plain PEG-PLA (T_g = 13°C) (Table 1). The T_g of the PEG block is too low to be detected, and the T_g of both PLA and PFMA blocks are probably very close to each other to be detected separately. Indeed, Li et al. reported the synthesis of PEG-PFMA block copolymers and found a T_g of -24.3 or -41.7 °C for the PEG block, and 19.5 °C for the PFMA block,[28] in agreement with our observations. Moreover, the glass transition of PEG-PLA-PFMA$_{20}$ appears less sharp than the others (supplementary material Figure S5), suggesting a stronger entanglement of polymer chains induced by a higher proportion of perfluoroalkyl units. This is consistent with the study of Li et al. where the glass transition of PFMA was observed only with the shorter PFMA block (28 fluorinated units) and not with increasing number of fluorinated units (36 and 38).[28]

A series of triblock copolymers containing a fluorinated block with a comb-like structure was therefore successfully synthesized using a combination of ROP and ATRP. This will allow studying the influence of the number of perfluoroalkyl pendant chains on polymers interfacial properties and on nanocapsules characteristics.

3.2. Polymers interfacial properties

The importance of polymer interfacial behavior during the formulation process of perfluorocarbon micro- and nanocapsules was highlighted in previous reports.[18,35,36] In particular, reducing the amount of PEG-PLGA in the formulation of PFOB nanocapsules led to local dewetting and expulsion of some PFOB droplets stabilized by sodium cholate.[18] The interfacial tension at the PFOB/organic phase interface was therefore measured with each triblock polymer (Figure 4). A reduction from 2.0 to 0.9-1.0 mN/m is observed upon addition of each PEG-PLA-PFMA$_x$ polymer at 25 mg/mL in methylene chloride, regardless of the number of fluorinated units, whereas no decrease is induced by addition of plain PEG-PLA (γ = 2.0 ± 0.3 mN/m). The profile as a function of time after the drop formation is also different between fluorinated polymers and the non-fluorinated one, showing a decrease of interfacial tension during the first few seconds with fluorinated polymers only (Figure 4). These results confirm that perfluoroalkyl pendant chains interact with PFOB and adsorb at the interface. Such finding is consistent with the reported fluorophilic character of perfluorinated chains, which usually form fluorous domains.[37–39] In a previous study, no reduction of interfacial tension could be observed with PLAs terminated by a linear fluorinated chain of length ranging from C_3F_7 to $C_{13}F_{27}$.[19] Adsorption of PEG-PLA-PFMA$_x$ polymers could potentially be favored by their higher fluorine content as compared to PLA-C_xF_{2x+1} polymers. However, the difference between PLA-$C_{13}F_{27}$ and PEG-PLA-PFMA$_5$ is not so important as compared to differences between all triblock polymers when taking into account the real degrees of polymerization: 25 mg of polymer contains ~45 µmol of fluorine for PLA-$C_{13}F_{27}$ and ~64 µmol for PEG-PLA-PFMA$_5$. This quantity then reaches ~100 µmol for PEG-PLA-PFMA$_{10}$ and ~194 µmol PEG-PLA-PFMA$_{20}$. Adsorption of triblock polymers is therefore probably favored by their comb-like architecture. In linear fluorinated PLAs, the fluorinated chain might be hidden by the PLA chain, whereas with the methacrylate backbone, the fluorinated

part is more rigid and more voluminous, making it more exposed and able to adsorb at the PFOB-solvent interface.

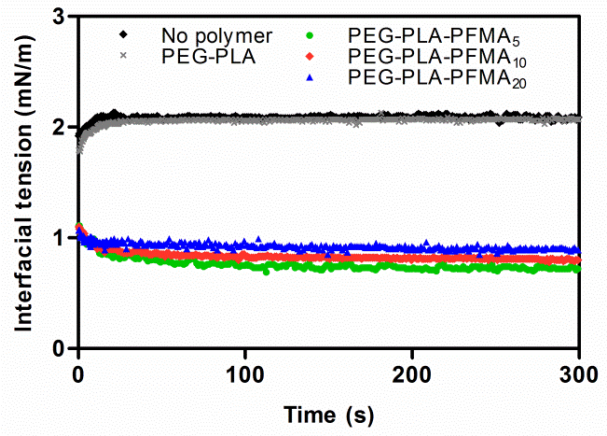

Polymer	Interfacial tension (mN/m)
No polymer	2.0 ± 0.3
PEG-PLA	2.0 ± 0.3
PEG-PLA-PFMA$_5$	0.9 ± 0.1
PEG-PLA-PFMA$_{10}$	0.9 ± 0.1
PEG-PLA-PFMA$_{20}$	1.0 ± 0.1

Figure 4. Interfacial tension measurements at the interface between PFOB and methylene chloride solutions of each polymer at 25 mg/mL with the pendant drop method: typical profiles as a function of time after the drop formation (top) and interfacial tension values at 200 s presented as mean ± SD (n > 6) (bottom).

3.3. PFOB nanocapsules: physical characterization

PFOB nanocapsules (NCs) were formulated using an emulsion evaporation process.[16,17] Since the objective was to reduce shell thickness, the initial amount of polymer in the organic phase was decreased (50, 30 and 20 mg), while keeping the amount of PFOB constant.

Size distribution and zeta potential

For a fixed polymer quantity, NCs mean hydrodynamic diameters are slightly larger with all PEG-PLA-PFMA$_x$ (117 – 147 nm) compared to PEG-PLA (113 – 131 nm) (Table 2). As observed with interfacial tension results, the number of fluorinated pendants does not seem to

have an influence on size and zeta potential. The polymer mass in the formulation is a more important parameter. Indeed, NCs formulated from 20 mg of polymer exhibit larger sizes than NCs from 50 and 30 mg, especially with the fluorinated polymers (136 – 147 nm at 20 mg compared to 117 – 119 nm at higher polymer amounts). For all polymers, the polydispersity (PDI) increases as the polymer quantity decreases (< 0.19 at 50 mg, > 0.28 at 20 mg), suggesting a wider size distribution at low polymer amount. This might arise from the presence of a second population of objects, such as non-encapsulated PFOB droplets, despite the addition of perfluorinated chains in the polymer, as previously observed with PLGA-PEG.[18] For all polymers, the zeta potential is negative and no significant difference is induced by the number of perfluoroalkyl chains (Table 2).

Table 2. Characterization of nanocapsules prepared from 50, 30 or 20 mg of each polymer. Data are presented as mean ± SD (n > 3) for d_H and ζ values.

	50 mg			30 mg			20 mg		
Polymer	**d_H (nm)**	**PDI**	**ζ (mV)**	**d_H (nm)**	**PDI**	**ζ (mV)**	**d_H (nm)**	**PDI**	**ζ (mV)**
PEG-PLA	113 ± 3	0.19	-17 ± 10	113 ± 3	0.22	-23 ± 9	131 ± 8	0.28	-29 ± 7
PEG-PLA-$PFMA_5$	117 ± 2	0.17	-15 ± 8	120 ± 5	0.24	-20 ± 4	140 ± 9	0.34	-30 ± 15
PEG-PLA-$PFMA_{10}$	116 ± 5	0.17	-15 ± 7	120 ± 6	0.26	-20 ± 5	136 ± 12	0.35	-21 ± 6
PEG-PLA-$PFMA_{20}$	119 ± 3	0.16	-15 ± 9	123 ± 2	0.26	-21 ± 5	147 ± 3	0.44	-23 ± 10

PFOB encapsulation efficiency

PFOB encapsulation efficiency in NCs was measured by ^{19}F NMR after freeze-drying to remove any non-encapsulated PFOB droplets remaining. As shown in Figure 5, more PFOB is encapsulated in PEG-PLA-$PFMA_x$ NCs compared to plain PEG-PLA NCs. When comparing to the PLA-PEG control, the encapsulation efficacy of PFOB is significantly higher for PEG-PLA-$PFMA_5$ and PEG-PLA-$PFMA_{10}$ ers for all initial masses of polymer but not for PEG-PLA-$PFMA_{20}$. The difference appears more important at low polymer amounts,

with 49-61% PFOB encapsulated in PEG-PLA-PFMA$_5$ and PEG-PLA-PFMA$_{10}$ NCs compared to 35% in PEG-PLA NCs at 30 mg, and 37-47% compared to 24% at 20 mg. Such results are consistent with interfacial tension measurements and demonstrate that fluorophilic interactions between PFOB and the perfluorinated units of the polymers allow entrapping more PFOB into the NCs. One can also observe that PFOB encapsulation efficiency is slightly lower with PEG-PLA-PFMA$_{20}$ compared to PEG-PLA-PFMA$_5$ and PEG-PLA-PFMA$_{10}$ (about 9 – 12% of difference). This could be due to a stronger self-association of the polymer with the largest fluorinated block of 20 pendants, reducing their ability to interact with PFOB as compared with shorter blocks of 5 – 10 fluorinated units.

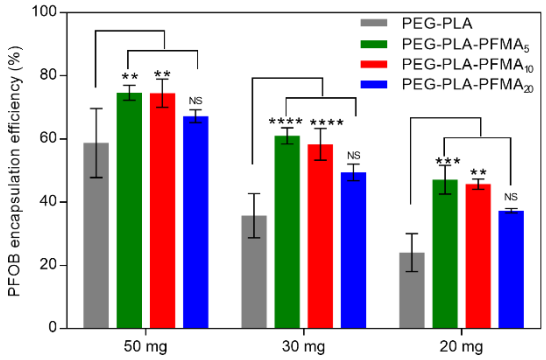

Figure 5. PFOB encapsulation efficiency in freeze-dried NCs. Results are presented as mean ± SD (n = 4). Statistical significance was analyzed using an ANOVA test: **** p<0.0001, *** p<0.001, ** p<0.01.

Nanocapsules morphology

Nanocapsules were then imaged by TEM with negative staining and cryo-TEM. In TEM images, one can observe mostly spherical objects with PEG-PLA (Figure 6A,B,C) whereas PEG-PLA-PFMA$_x$ NCs exhibit more heterogeneous morphologies (Figure 6 and supplementary material S6 to S9). Indeed, capsules appear less spherical and a lot of broken capsules can be observed at low polymer amounts (Figure 6E,F,H,I,K,L). These broken

capsules, which were neither observed in plain PEG-PLA samples nor for NCs made from 50 mg of PEG-PLA-PFMA$_x$, are sometimes very large (up to 1 µm diameter, see supplementary material). Such finding is surprising since NCs are filtered on 0.45 µm after the emulsion evaporation process. These objects might be very deformable to pass through the filter, and might be broken because of the filtration or because they are under vacuum during TEM observation. These large capsules can therefore explain the high PDI values observed at low fluorinated polymer amounts (Table 2).

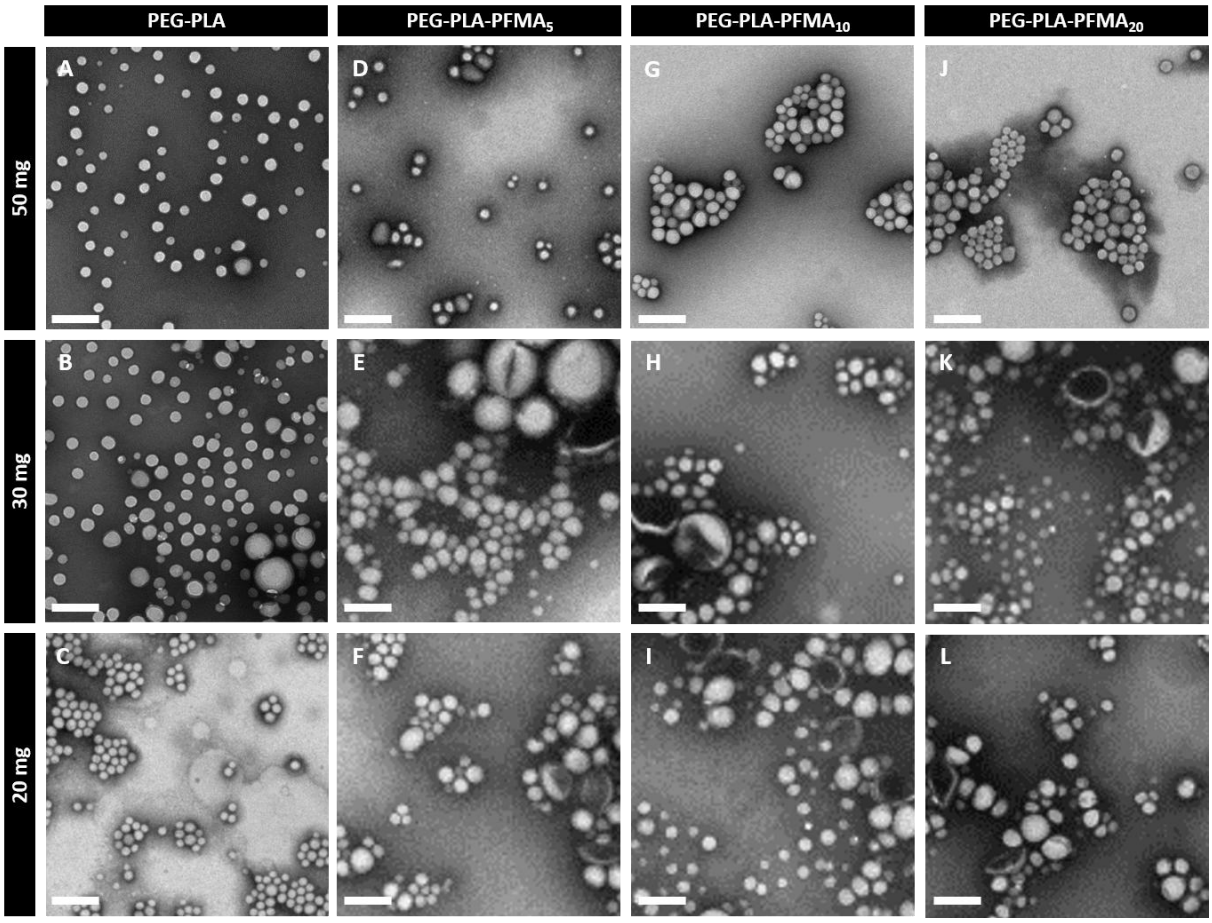

Figure 6. TEM images of formulated NCs with negative staining (scale bars = 200 nm). Additional images are shown in supplementary material.

Cryo-TEM images allow distinguishing the dark PFOB core, with high electronic density, from the lighter polymeric shell (Figure 7 and supplementary material S6 to S9). NCs also present a white meniscus in the core, due to rapid freezing, which causes solidification and

shrinking of PFOB. PFOB therefore does not fill entirely the shell cavity anymore as observed previously.[18,19,40] One can observe that NCs morphology is strongly influenced by the number of fluorinated chains and the amount of polymer used for formulation. Indeed, all PEG-PLA NCs possess a spherical core-shell structure (Figure 7A,B,C), whereas the presence of five perfluoroalkyl chains induces the formation of some elongated NCs with a non-centered PFOB core looking like sunny-side up eggs (shown by red stars in Figure 7D,E). Such elongated morphology had already been observed with COOH-PEG-PLA NCs. This was attributed to an interfacial instability due to electrostatic repulsions between deprotonated carboxy functions leading to an increase of the total surface area.[30] Comparatively, with PEG-PLA-PFMA$_5$, we can imagine that the incompatibility between the various blocks may force the chains to adopt a particular conformation leading to an increase of the total surface area. The same type of morphologies (shown by red stars) is observed with 50 and 30 mg of PEG-PLA-PFMA$_{10}$, but with additional dark domains (shown by red arrows) in the same object (Figure 7G,H), which correspond either to other PFOB cores, or to fluorinated rich domains formed by aggregation of the perfluoroalkyl chains of the polymer.[41] PEG-PLA-PFMA$_{20}$ leads to NCs with 2 or 3 distinct PFOB cores at high polymer amounts, as shown by blue circles in Figure 7J,K. Such multi-core structures are probably favored by strong interactions between PFOB and perfluoroalkyl pendants. However, at 20 mg of each fluorinated polymer, although morphologies are still a bit heterogeneous within a same sample, one can observe a majority of capsules with a single centered PFOB core and a thin shell (Figure 7F,I,L). Interestingly, some are not perfectly spherical and seem ellipsoidal/elongated (shown by yellow triangles), which may indicate different mechanical properties. In this type of capsules, the PFOB core is not spherical and the shell thickness is homogeneous within the whole capsule, which is different from the other elongated NCs observed at higher polymer amounts.

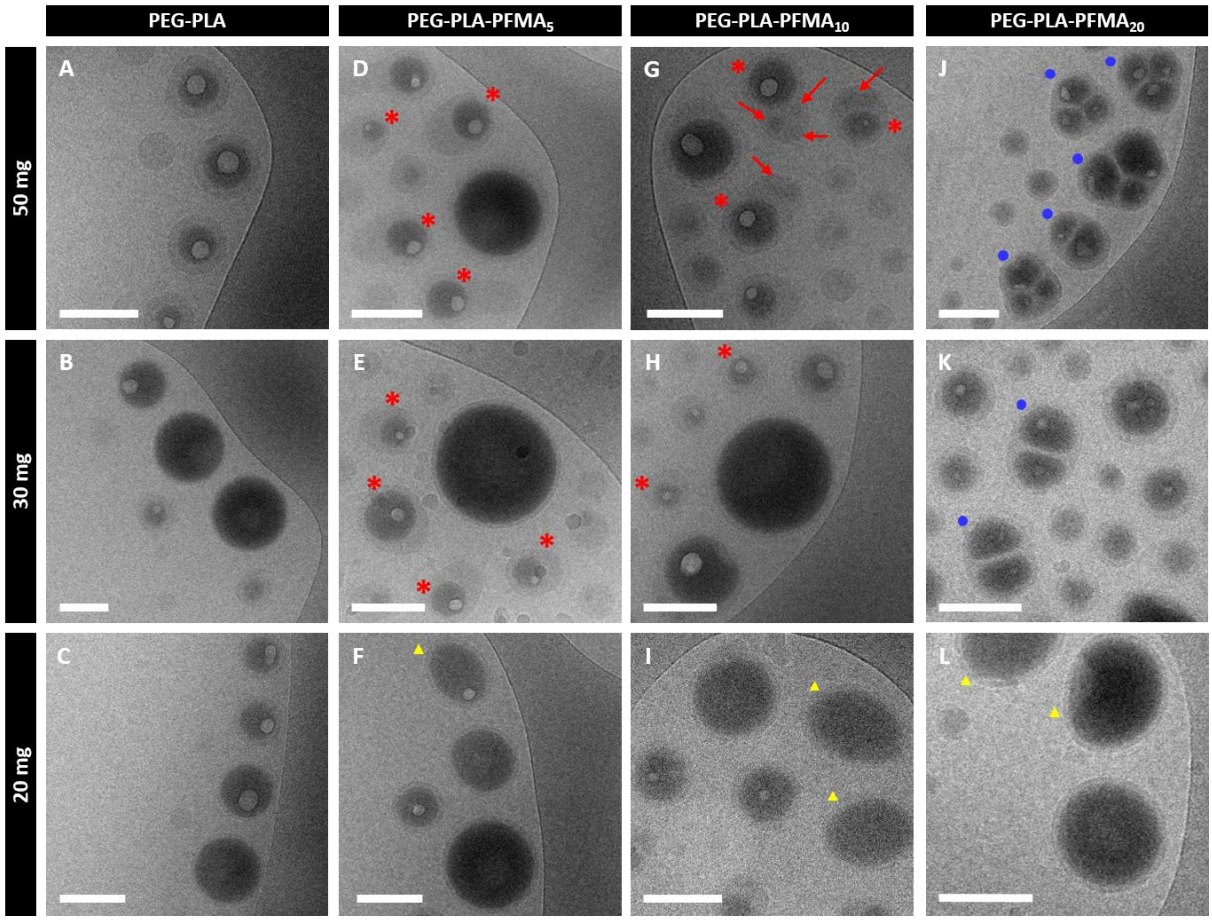

Figure 7. Cryo-TEM images of formulated NCs (scale bars = 100 nm). Additional images are given in supplementary material. Red stars show elongated NCs with a non-centered spherical PFOB core at high amounts of PEG-PLA-PFMA$_5$ and PEG-PLA-PFMA$_{10}$. In the case of PEG-PLA-PFMA$_{10,}$ this type of elongated NCs also possesses additional darker domains shown by red arrows. Blue circles show NCs with 2 or 3 distinct PFOB cores. Yellow triangles show ellipsoidal NCs with a single non-spherical PFOB core and a shell thickness homogeneous within the same capsule.

Shell thickness

Small Angle Neutron Scattering (SANS) was used to statistically determine shell thickness. We focused on PEG-PLA-PFMA$_5$ and PEG-PLA-PFMA$_{10}$ which showed better PFOB encapsulation efficiency and higher solubility in methylene chloride than PEG-PLA-PFMA$_{20}$. NCs were resuspended in the appropriate mixture of H_2O and D_2O to match the scattering

length density of the PFOB core and allow focusing on the polymeric shell. Scattered intensity curves were fitted with the vesicle model, assuming a log-normal distribution for both shell thickness and core radius. One example of a satisfying fit and the best fit parameters obtained for shell thickness are represented in Figure 8. Fitted curves and numerical values of shell thickness and core radius are given in supplementary material (Figure S10 and Table S1). Mean PFOB core radii are all in the same range (53 – 56 nm) with a high polydispersity, in agreement with DLS measurements. The mean thickness of PEG-PLA NCs is not impacted by the amount of polymer, with values between 16 and 14.5 nm. However, with fluorinated triblock polymers, the mean thickness is decreasing down to 13.5 nm and 11 nm for 20 mg of PEG-PLA-PFMA$_5$ and PEG-PLA-PFMA$_{10}$, respectively, as compared with 50 and 30mg polymer where no difference can be observed. This decrease is meaningful as the precision of SANS fitting is on the 1-2 nm order. A high polydispersity is nevertheless observed for all samples, especially for NCs made from higher fluorinated polymer amounts. This can be attributed to PFOB cores not being always well centered as seen on cryo-TEM images.

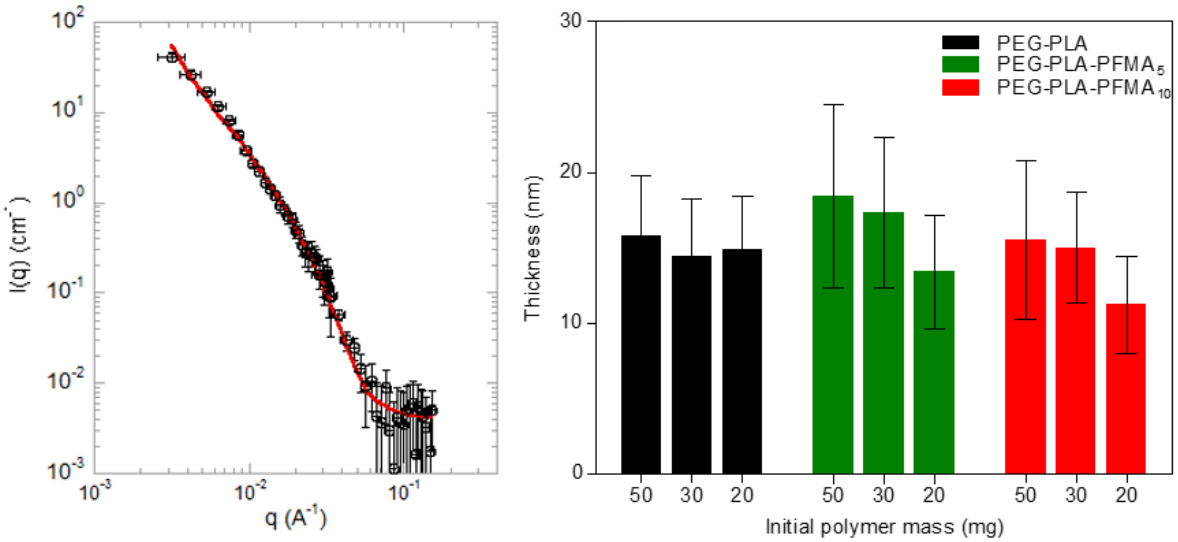

Figure 8. Experimental scattered intensity curve (black circles) of NCs made from 20 mg PEG-PLA-PFMA$_{10}$ in PFOB matching condition fitted with the vesicle model (red line) (left)

and shell thickness values of NCs determined by fitting with the vesicle model (mean ± SD) (right).

3.4. Cytotoxicity studies

The biological inertness of perfluorocarbons is well documented.[42] Nevertheless, perfluoroalkyl moieties are often associated to a certain toxicity due to their low excretion profiles and prolonged retention in the organism, especially linear perfluorinated chains longer than eight carbons.[43–45] Therefore the potential cytotoxicity of PEG-PLA-PFMA$_x$ NCs was investigated using an MTT assay on two representative cell types. Human umbilical vein endothelial cells (HUVEC) were chosen for their high sensitivity and rapid response to external stimuli which make them a widely used *in vitro* model for polymer cytotoxicity evaluation.[46] J774.A1 cells play a key role in phagocytosis and were chosen to highlight the possible toxicity of NCs after being engulfed by macrophages. At both 24 and 72h incubation times, cell viability of HUVEC slightly decreases as NCs concentration increases, but remains above 70% until 1 mg/mL, and above 50% at 10 mg/mL, with no difference between the polymers (Figure 9A and Figure S11A). Regarding J774.A1, cellular viability remains above 80% until 1 mg/mL at both incubation times. A strong viability decrease down to 45% after 24h and 20% after 72h is observed at 10 mg/mL, but this high concentration is unlikely to be reached in vivo (Figure 9A and Figure S11A). For both cell types and both incubation times, the perfluoroalkyl chains do not induce any specific toxicity in comparison to plain PEG-PLA, with no influence of the number of perfluoroalkyl chains. These results concur with reports from Koda et al. on the low toxicity of an amphiphilic fluorous random copolymer containing PEG and C_8F_{17} pendants.[34]

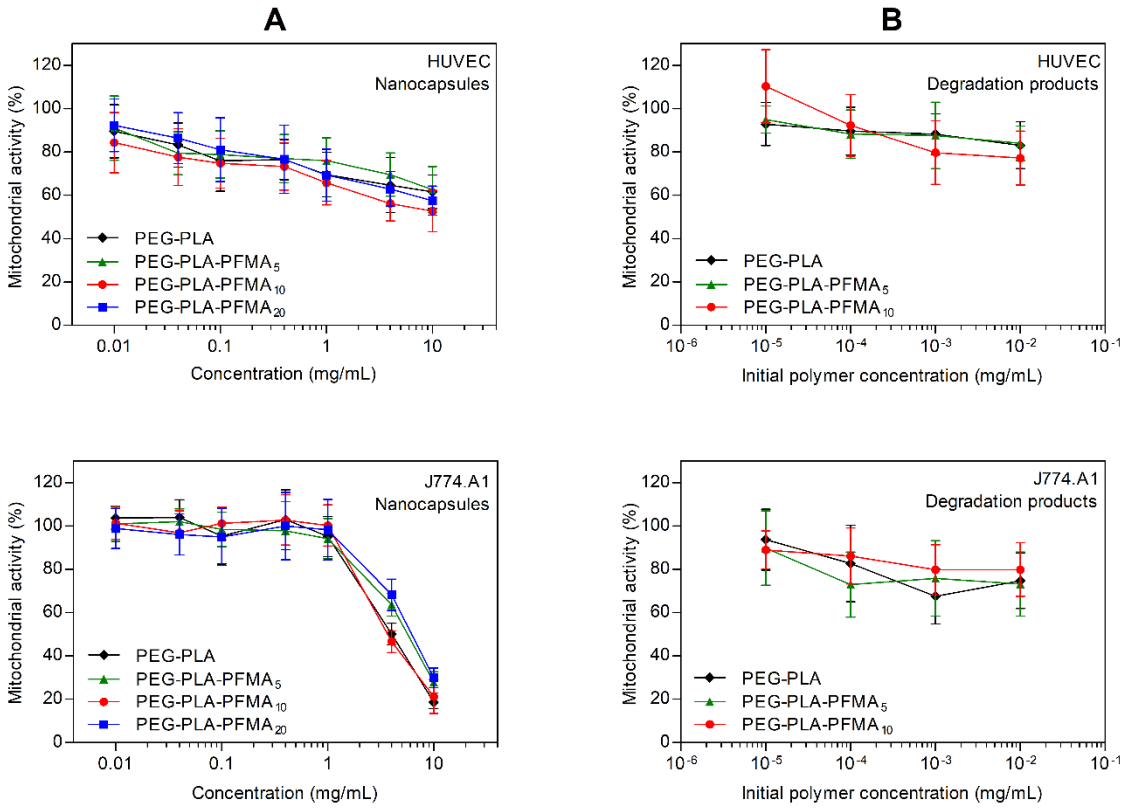

545

546 **Figure 9**1. Viability assays on HUVEC (top) and J774.A1 (bottom) cell lines after 72h
547 incubation with nanocapsules (A) or polymers degradation products (B). Results are presented
548 as mean ± SD (n = 3).

549 PEG-PLA diblock copolymer is well known to be degradable into non-toxic products (lactic
550 acid and polyethylene glycol). However, toxicity of the remaining short PFMA block after
551 degradation of the triblock copolymers must be investigated. Accelerated hydrolytic
552 degradations of PEG-PLA-PFMA$_5$, PEG-PLA-PFMA$_{10}$, and PEG-PLA as control, were
553 carried out in basic conditions. The *in vitro* cytotoxicity of degradation products was then
554 evaluated using an MTT assay on the same cell lines as for NCs. Due to insolubility issues,
555 only low concentrations could be tested (maximum 0.01 mg/mL of initial polymer). In this
556 range of concentrations, high HUVEC cellular viabilities (> 70%) were observed at both
557 incubation times (Figure 9B and Figure S11B). J774.A1 cells show a slightly higher
558 sensitivity depending on the incubation time, with cell viabilities above 87% after 24h and

above 67% after 72h. Within experimental error, no significant differences between polymers can be observed for both cell types, indicating an absence of obvious toxicity arising from fluorinated degradation products (Figure 9B and Figure S11B). These results are encouraging and additional *in vivo* studies will be required to evaluate the potential toxicity arising from a prolonged exposure to the degradation products.

3.5. *In vitro* ultrasound measurements

Finally, the acoustic response of NCs made from 30 and 20 mg polymer was evaluated *in vitro* at 5 MHz. Figure 10A presents the ultrasound scattered intensities measured at fundamental frequency and subtracted by the background level produced by Milli-Q water. No non-linear response could indeed be detected with our capsules, in agreement with previous studies showing the absence of nonlinear scattering with nano-sized agents.[47,48] At 30 mg polymer, all samples did not yield an ultrasound signal much higher than the background (intensity < 0.9 x 10^3 arbitrary units, a.u.). However, at 20 mg polymer, the ultrasound scattered intensity increases with the number of fluorinated pendant chains, from 1.4 x 10^3 a.u. with plain PEG-PLA to 2.5 x 10^3 a.u. with PEG-PLA-$PFMA_5$ and 5.3 x 10^3 a.u. with PEG-PLA-$PFMA_{10}$. Such enhancement probably arises from several contributions which are summarized in Table 3. As shown by De Jong et al., the scattering cross section of a particle is defined as $SCS = \frac{4\pi}{9} k^4 R^6 \left[\left(\frac{\kappa_d - \kappa}{\kappa}\right)^2 + \frac{3}{4}\frac{(\rho_d - \rho)^2}{(\rho_d + \rho)^2}\right]$ where k is the wavenumber, R is the radius of the particle, κ_d and κ the compressibilities of respectively the particle and the medium, ρ_d and ρ the densities of respectively the particle and the medium.[49] A contrast agent will therefore backscatter ultrasound waves more effectively if its radius is larger and if its physical properties (compressibility and density) differ a lot from the ones of the surrounding medium. Here, the slight diameter difference (up to 27 nm) could hardly be considered

583 responsible for the higher efficacy in scattering ultrasound. One of the main contribution is
584 probably the reduction of shell thickness (down to 13.5 nm for PEG-PLA-PFMA$_5$ and 11 nm
585 for PEG-PLA-PFMA$_{10}$) which may increase the capsules compressibility and echogenicity as
586 previously observed.[15] Indeed, AFM indentation experiments performed on PFOB
587 microcapsules have shown that a thinner shell leads to overall softer capsules.[50] Moreover,
588 higher encapsulated PFOB contents and higher amounts of fluorinated chains in the polymers
589 both increase capsule density and strengthen the difference of acoustic impedance with the
590 surrounding medium, as previously observed with linear fluorinated PLAs.[19] Although the
591 quantity of PFOB and fluorinated chains is also high in samples made from 30 mg of PEG-
592 PLA-PFMA$_5$ and PEG-PLA-PFMA$_{10}$, these two samples possess a larger shell thickness (>
593 15 nm) and a different morphology with a non-centered PFOB core (Figure 10B). The
594 observed differences in capsules morphology are probably related to some differences in their
595 mechanical properties which impact their response to ultrasound waves. AFM indentation
596 experiments should be performed in the future to relate mechanical properties and ultrasound
597 signal.

598 Nanocapsules made from 20 mg of fluorinated triblock polymers therefore appear as
599 promising UCAs. Although the measured ultrasound scattered intensities were still lower that
600 with SonoVue® microbubbles (16.5 x 10^3 a.u.) due to their large radius (20-fold larger than
601 NCs) and gaseous core, these NCs have greater potential to accumulate into the tumors by the
602 EPR effect and allow contrast ultrasound imaging of tumors.

A

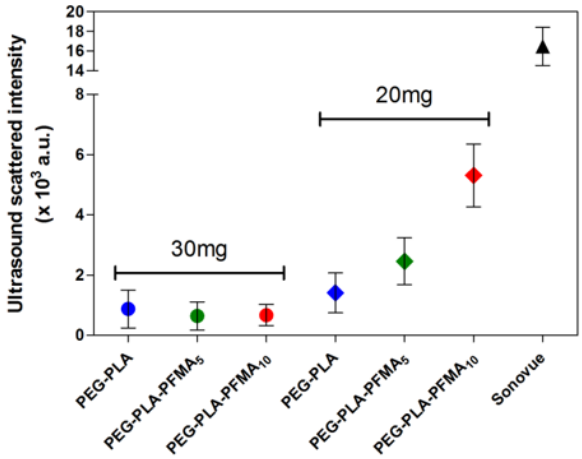

B

Initial polymer mass	30 mg			20 mg		
Polymer	PEG-PLA	PEG-PLA-PFMA$_5$	PEG-PLA-PFMA$_{10}$	PEG-PLA	PEG-PLA-PFMA$_5$	PEG-PLA-PFMA$_{10}$
Main morphology						
mean d_H (nm)	113	120	120	131	140	136
mean T (nm)	14.5	17.5	15	15	13.5	11
PFOB (µmol)	6.9	11.8	11.3	7.0	13.7	13.3
C_8F_{17} chains (µmol)	0.0	0.7	1.2	0.0	0.7	1.2

Figure 10. (A) Ultrasound scattered intensity by NCs resuspended at 5 mg/mL made from 30 mg (circles) and 20 mg (diamonds) of each polymer and by Sonovue microbubbles (dark triangle) as positive control. Results are presented as mean ± SEM (n > 9). (B) Table summarizing NCs characteristics which could account for differences of ultrasound scattering: simplified representation of their morphology, mean hydrodynamic diameter (d_H), mean shell thickness (T), PFOB quantity and C_8F_{17} chains quantity contained in 1 mL of formulation resuspended at a final polymer concentration of 5 mg/mL for ultrasound measurements.

4. Conclusion

Triblock PEG-PLA-PFMA polymers with distinct lengths of PFMA block (5, 10 or 20 fluorinated pendant chains) were successfully synthesized and were shown to adsorb at the PFOB/methylene chloride interface. These favorable fluorous interactions led to an increase of the PFOB encapsulation efficiency into nanocapsules made of fluorinated polymers compared to plain PEG-PLA. The morphology of the nanocapsules was strongly influenced by the number of perfluorinated chains and the amount of polymer used for formulation: capsules with several PFOB cores or fluorinated-rich domains are obtained at high polymer amount, while a single PFOB core and a thinner shell are observed at low polymer amount. SANS measurements confirmed the observed reduction of mean shell thickness down to 11 nm with PEG-PLA-PFMA$_{10}$, which led to a 3.7-fold higher *in vitro* ultrasound response at 5 MHz compared to plain PEG-PLA nanocapsules. Finally, no *in vitro* cytotoxicity was induced by both the fluorinated polymers and their degradation products. Results are encouraging, and future work will consist in performing *in vivo* studies to confirm the potential of these PEGylated/fluorinated nanocapsules to be used as ultrasound contrast agents for tumor imaging.

5. Supporting information

Supporting information is available: scheme of the experimental set up for in vitro ultrasound measurements, ^{1}H NMR spectra of PEG-PLA and PEG-PLA-Br, SEC chromatograms, DLS of polymers in methylene chloride and chloroform, DSC thermograms, additional TEM and cryo-TEM images, SANS curves fitting, cytotoxicity results after 24h incubation, DLS curves of NCs (correlation and distribution functions).

6. Acknowledgements

Authors would like to thank Mehrez Sghaier and Najet Yagoubi from Laboratoire Matériaux et Santé (EA401, Univ. Paris-Sud) for DSC experiments, Flora Lefebvre for some NMR measurements and Stéphanie Denis (Institut Galien Paris-Sud) for her help with cell culture. This work has been supported by the Région Ile-de-France in the framework of DIM Nano-K. The present work has benefited also from the core facilities of Imagerie- Gif, (http://www.i2bc.paris- saclay.fr), member of IBiSA (http://www.ibisa.net), supported by "France- BioImaging" (ANR- 10- INBS- 04- 01), and the Labex "Saclay Plant Science" (ANR- 11- IDEX- 0003- 02). SANS analysis was performed using SasView software, originally developed by the DANSE project under NSF award DMR-0520547. Authors acknowledge financial support from ANR (Investissements d'Avenir, Nanobiotechnologies, ANR-10-NANO-06-04). Institut Galien Paris-Sud is a member of the Laboratory of Excellence LERMIT supported by a grant from ANR (ANR-10-LABX-33).

649 References

650 (1) Boissenot, T.; Bordat, A.; Fattal, E.; Tsapis, N. Ultrasound-Triggered Drug Delivery for Cancer
651 Treatment Using Drug Delivery Systems: From Theoretical Considerations to Practical
652 Applications. *Journal of Controlled Release*. 2016, pp 144–163.

653 (2) Schutt, E. G.; Klein, D. H.; Mattrey, R. M.; Riess, J. G. Injectable Microbubbles as Contrast Agents for
654 Diagnostic Ultrasound Imaging: The Key Role of Perfluorochemicals. *Angew. Chemie-International*
655 *Ed.* **2003**, *42* (28), 3218–3235.

656 (3) Paefgen, V.; Doleschel, D.; Kiessling, F. Evolution of Contrast Agents for Ultrasound Imaging and
657 Ultrasound-Mediated Drug Delivery. *Front. Pharmacol.* **2015**, *6*.

658 (4) Schneider, M.; Arditi, M.; Barrau, M. B.; Brochot, J.; Broillet, A.; Ventrone, R.; Yan, F. Br1 - a New
659 Ultrasonographic Contrast Agent Based on Sulfur Hexafluoride-Filled Microbubbles. *Invest. Radiol.*
660 **1995**, *30* (8), 451–457.

661 (5) Fisher, N. G.; Christiansen, J. P.; Leong-Poi, H.; Jayaweera, A. R.; Lindner, J. R.; Kaul, S. Myocardial
662 and Microcirculatory Kinetics of BR14, a Novel Third-Generation Intravenous Ultrasound Contrast
663 Agent. *J. Am. Coll. Cardiol.* **2002**, *39* (3), 530–537.

664 (6) Lindner, J. R. Microbubbles in Medical Imaging: Current Applications and Future Directions. *Nat.*
665 *Rev. Drug Discov.* **2004**, *3* (6), 527–532.

666 (7) Abou-Saleh, R. H.; Peyman, S. A.; Johnson, B. R. G.; Marston, G.; Ingram, N.; Bushby, R.; Coletta, P. L.;
667 Markham, A. F.; Evans, S. D. The Influence of Intercalating Perfluorohexane into Lipid Shells on
668 Nano and Microbubble Stability. *Soft Matter* **2016**, *12* (34), 7223–7230.

669 (8) Yuan, F.; Dellian, M.; Fukumura, D.; Leunig, M.; Berk, D. A.; Torchilin, V. P.; Jain, R. K. Vascular-
670 Permeability in a Human Tumor Xenograft - Molecular-Size Dependence and Cutoff Size. *Cancer*
671 *Res.* **1995**, *55* (17), 3752–3756.

672 (9) Leroy, V.; Norisuye, T. Investigating the Existence of Bulk Nanobubbles with Ultrasound.
673 *Chemphyschem* **2016**, *17* (18), 2787–2790.

(10) Cosco, D.; Fattal, E.; Fresta, M.; Tsapis, N. Perfluorocarbon-Loaded Micro and Nanosystems for Medical Imaging: A State of the Art. *J. Fluor. Chem.* **2015**, *171*, 18–26.

(11) El-Sherif, D. M.; Wheatley, M. A. Development of a Novel Method for Synthesis of a Polymeric Ultrasound Contrast Agent. *J. Biomed. Mater. Res. A* **2003**, *66* (2), 347–355.

(12) Chlon, C.; Guedon, C.; Verhaagen, B.; Shi, W. T.; Hall, C. S.; Lub, J.; Bohmer, M. R. Effect of Molecular Weight, Crystallinity, and Hydrophobicity on the Acoustic Activation of Polymer-Shelled Ultrasound Contrast Agents. *Biomacromolecules* **2009**, *10* (5), 1025–1031.

(13) Yang, P.; Li, D.; Jin, S.; Ding, J.; Guo, J.; Shi, W. B.; Wang, C. C. Stimuli-Responsive Biodegradable Poly(Methacrylic Acid) Based Nanocapsules for Ultrasound Traced and Triggered Drug Delivery System. *Biomaterials* **2014**, *35* (6), 2079–2088.

(14) Sanna, V.; Pintus, G.; Bandiera, P.; Anedda, R.; Punzoni, S.; Sanna, B.; Migaleddu, V.; Uzzau, S.; Sechi, M. Development of Polymeric Microbubbles Targeted to Prostate-Specific Membrane Antigen as Prototype of Novel Ultrasound Contrast Agents. *Mol. Pharm.* **2011**, *8* (3), 748–757.

(15) Pisani, E.; Tsapis, N.; Galaz, B.; Santin, M.; Berti, R.; Taulier, N.; Kurtisovski, E.; Lucidarme, O.; Ourevitch, M.; Doan, B. T.; et al. Perfluorooctyl Bromide Polymeric Capsules as Dual Contrast Agents for Ultrasonography and Magnetic Resonance Imaging. *Adv. Funct. Mater.* **2008**, *18* (19), 2963–2971.

(16) Diou, O.; Tsapis, N.; Giraudeau, C.; Valette, J.; Gueutin, C.; Bourasset, F.; Zanna, S.; Vauthier, C.; Fattal, E. Long-Circulating Perfluorooctyl Bromide Nanocapsules for Tumor Imaging by (FMRI)-F-19. *Biomaterials* **2012**, *33* (22), 5593–5602.

(17) Pisani, E.; Tsapis, N.; Paris, J.; Nicolas, V.; Cattel, L.; Fattal, E. Polymeric Nano/Microcapsules of Liquid Perfluorocarbons for Ultrasonic Imaging: Physical Characterization. *Langmuir* **2006**, *22* (9), 4397–4402.

(18) Diou, O.; Brulet, A.; Pehau-Arnaudet, G.; Morvan, E.; Berti, R.; Astafyeva, K.; Taulier, N.; Fattal, E.; Tsapis, N. PEGylated Nanocapsules of Perfluorooctyl Bromide: Mechanism of Formation, Influence of Polymer Concentration on Morphology and Mechanical Properties. *Colloids Surf B Biointerfaces*

2016, *146*, 762–769.

(19) Houvenagel, S.; Picheth, G.; Dejean, C.; Brulet, A.; Chenneviere, A.; Couture, O.; Huang, N.; Moine, L.; Tsapis, N. End-Chain Fluorination of Polyesters Favors Perfluorooctyl Bromide Encapsulation into Echogenic PEGylated Nanocapsules. *Polym. Chem.* **2017**, *8* (16), 2559–2570.

(20) Berlepsch, H. v.; Böttcher, C.; Skrabania, K.; Laschewsky, A. Complex Domain Architecture of Multicompartment Micelles from a Linear ABC Triblock Copolymer Revealed by Cryogenic Electron Tomography. *Chem. Commun.* **2009**, *0* (17), 2290.

(21) Skrabania, K.; Laschewsky, A.; Berlepsch, H. v.; Böttcher, C. Synthesis and Micellar Self-Assembly of Ternary Hydrophilic–Lipophilic–Fluorophilic Block Copolymers with a Linear PEO Chain. *Langmuir* **2009**, *25* (13), 7594–7601.

(22) Skrabania, K.; Berlepsch, H. v.; Böttcher, C.; Laschewsky, A. Synthesis of Ternary, Hydrophilic–Lipophilic–Fluorophilic Block Copolymers by Consecutive RAFT Polymerizations and Their Self-Assembly into Multicompartment Micelles. *Macromolecules* **2010**, *43* (1), 271–281.

(23) Kaberov, L. I.; Verbraeken, B.; Hruby, M.; Riabtseva, A.; Kovacik, L.; Kereïche, S.; Brus, J.; Stepanek, P.; Hoogenboom, R.; Filippov, S. K. Novel Triphilic Block Copolymers Based on Poly(2-Methyl-2-Oxazoline)– Block –poly(2-Octyl-2-Oxazoline) with Different Terminal Perfluoroalkyl Fragments: Synthesis and Self-Assembly Behaviour. *Eur. Polym. J.* **2017**, *88*, 645–655.

(24) Kaberov, L. I.; Verbraeken, B.; Riabtseva, A.; Brus, J.; Talmon, Y.; Stepanek, P.; Hoogenboom, R.; Filippov, S. K. Fluorinated 2-Alkyl-2-Oxazolines of High Reactivity: Spacer-Length-Induced Acceleration for Cationic Ring-Opening Polymerization As a Basis for Triphilic Block Copolymer Synthesis. *ACS Macro Lett.* **2018**, *7* (1), 7–10.

(25) NIJENHUIS, A. J.; GRIJPMA, D. W.; PENNINGS, A. J. Lewis Acid-Catalyzed Polymerization of L-Lactide - Kinetics and Mechanism of the Bulk-Polymerization. *Macromolecules* **1992**, *25* (24), 6419–6424.

(26) Spasova, M.; Mespouille, L.; Coulembier, O.; Paneva, D.; Manolova, N.; Rashkov, I.; Dubois, P. Amphiphilic Poly(D- or L-Lactide)-b-Poly(N,N-Dimethylamino-2-Ethyl Methacrylate) Block Copolymers: Controlled Synthesis, Characterization, and Stereocomplex Formation.

Biomacromolecules **2009**, *10* (5), 1217–1223.

(27) Zhao, Y.; Shuai, X.; Chen, C.; Xi, F. Synthesis of Star Block Copolymers from Dendrimer Initiators by Combining Ring-Opening Polymerization and Atom Transfer Radical Polymerization. *Macromolecules* **2004**, *37* (24), 8854–8862.

(28) Li, H.; Gu, W. Y.; Li, L.; Zhang, Y. M.; Russell, T. P.; Coughlin, E. B. Synthesis of Semicrystalline/Fluorinated Side-Chain Crystalline Block Copolymers and Their Bulk and Thin Film Nanoordering. *Macromolecules* **2013**, *46* (10), 3737–3745.

(29) Henderson, T. J. Quantitative NMR Spectroscopy Using Coaxial Inserts Containing a Reference Standard: Purity Determinations for Military Nerve Agents. *Anal. Chem.* **2002**, *74* (1), 191–198.

(30) Diou, O.; Fattal, E.; Delplace, V.; Mackiewicz, N.; Nicolas, J.; Meriaux, S.; Valette, J.; Robic, C.; Tsapis, N. RGD Decoration of PEGylated Polyester Nanocapsules of Perfluorooctyl Bromide for Tumor Imaging: Influence of Pre or Post-Functionalization on Capsule Morphology. *Eur. J. Pharm. Biopharm.* **2014**, *87* (1), 170–177.

(31) Brulet, A.; Lairez, D.; Lapp, A.; Cotton, J. P. Improvement of Data Treatment in Small-Angle Neutron Scattering. *J. Appl. Crystallogr.* **2007**, *40*, 165–177.

(32) Sasview software.

(33) Koda, Y.; Terashima, T.; Sawamoto, M. Fluorinated Microgel Star Polymers as Fluorous Nanocapsules for the Encapsulation and Release of Perfluorinated Compounds. *Polym. Chem.* **2015**, *6* (31), 5663–5674.

(34) Koda, Y.; Terashima, T.; Sawamoto, M.; Maynard, H. D. Amphiphilic/Fluorous Random Copolymers as a New Class of Non-Cytotoxic Polymeric Materials for Protein Conjugation. *Polym. Chem.* **2015**, *6*, 240–247.

(35) Pisani, E.; Fattal, E.; Paris, J.; Ringard, C.; Rosilio, V.; Tsapis, N. Surfactant Dependent Morphology of Polymeric Capsules of Perfluorooctyl Bromide: Influence of Polymer Adsorption at the Dichloromethane-Water Interface. *J. Colloid Interface Sci.* **2008**, *326* (1), 66–71.

(36) Mousnier, L.; Huang, N.; Morvan, E.; Fattal, E.; Tsapis, N. Influence of Polymer End-Chemistry on the

Morphology of Perfluorohexane Polymeric Microcapsules Intended as Ultrasound Contrast Agents. *Int. J. Pharm.* **2014**, *471* (1–2), 10–17.

(37) Riess, J. G. Fluorous Micro- and Nanophases with a Biomedical Perspective. *Tetrahedron* **2002**, *58* (20), 4113–4131.

(38) Krafft, M. P.; Riess, J. G. Chemistry, Physical Chemistry, and Uses of Molecular Fluorocarbon-Hydrocarbon Diblocks, Triblocks, and Related Compounds-Unique "Apblar" Components for Self-Assembled Colloid and Interface Engineering. *Chem. Rev.* **2009**, *109* (5), 1714–1792.

(39) Hillmyer, M. A.; Lodge, T. P. Synthesis and Self-Assembly of Fluorinated Block Copolymers. *J. Polym. Sci. Part a-Polymer Chem.* **2002**, *40* (1), 1–8.

(40) Boissenot, T.; Fattal, E.; Bordat, A.; Houvenagel, S.; Valette, J.; Chacun, H.; Gueutin, C.; Tsapis, N. Paclitaxel-Loaded PEGylated Nanocapsules of Perfluorooctyl Bromide as Theranostic Agents. *Eur. J. Pharm. Biopharm.* **2016**, *108*, 136–144.

(41) Li, Z.; Kesselman, E.; Talmon, Y.; Hillmyer, M. A.; Lodge, T. P. Multicompartment Micelles from ABC Miktoarm Stars in Water. *Science (80-.).* **2004**, *306* (5693), 98–101.

(42) Krafft, M. P.; Riess, J. G. Perfluorocarbons: Life Sciences and Biomedical Uses - Dedicated to the Memory of Professor Guy Ourisson, a True RENAISSANCE Man. *J. Polym. Sci. Part a-Polymer Chem.* **2007**, *45* (7), 1185–1198.

(43) Riess, J. G. Highly Fluorinated Amphiphilic Molecules and Self-Assemblies with Biomedical Potential. *Curr. Opin. Colloid Interface Sci.* **2009**, *14* (5), 294–304.

(44) Zaggia, A.; Ameduri, B. Recent Advances on Synthesis of Potentially Non-Bioaccumulable Fluorinated Surfactants. *Curr. Opin. Colloid Interface Sci.* **2012**, *17* (4), 188–195.

(45) Barmentlo, S. H.; Stel, J. M.; van Doom, M.; Eschauzier, C.; de Voogt, P.; Kraak, M. H. S. Acute and Chronic Toxicity of Short Chained Perfluoroalkyl Substances to Daphnia Magna. *Environ. Pollut.* **2015**, *198*, 47–53.

(46) Kirkpatrick, C. J.; Otto, M.; Van Kooten, T.; Krump, V.; Kriegsmann, J.; Bittinger, F. Endothelial Cell Cultures as a Tool in Biomaterial Research. *J. Mater. Sci. Mater. Med.* **1999**, *10*, 589–594.

(47) Hughes, M. S.; Marsh, J. N.; Hall, C. S.; Fuhrhop, R. W.; Lacy, E. K.; Lanza, G. M.; Wickline, S. A. Acoustic Characterization in Whole Blood and Plasma of Site-Targeted Nanoparticle Ultrasound Contrast Agent for Molecular Imaging. *J. Acoust. Soc. Am.* **2005**, *117* (2), 964.

(48) Couture, O.; Bevan, P. D.; Cherin, E.; Cheung, K.; Burns, P. N.; Foster, F. S. Investigating Perfluorohexane Particles with High-Frequency Ultrasound. *Ultrasound Med. Biol.* **2006**, *32* (1), 73–82.

(49) de Jong, N.; Ten Cate, F. J.; Lancée, C. T.; Roelandt, J. R. T. C.; Bom, N. Principles and Recent Developments in Ultrasound Contrast Agents. *Ultrasonics* **1991**, *29* (4), 324–330.

(50) Sarrazin, B.; Tsapis, N.; Mousnier, L.; Taulier, N.; Urbach, W.; Guenoun, P. AFM Investigation of Liquid-Filled Polymer Microcapsules Elasticity. *Langmuir* **2016**, *32* (18).

790 **Table of Contents graphic**

791